Development of a Flexible Robotic System for Multiscale Applications of Micro/Nanoscale Manipulation and Assembly

Hui Xie, *Member, IEEE*, and Stéphane Régnier

***Abstract*—A flexible robotic system (FRS) developed for multiscale manipulation and assembly from nanoscale to microscale is presented. This system is based on the principle of atomic force microscopy and comprises two individually functionalized cantilevers. After reconfiguration, the robotic system could be used for pick-and-place manipulation from nanoscale to the scale of several micrometers, as well as parallel imaging/nanomanipulation. Flexibilities and manipulation capabilities of the developed system were validated by pick-and-place manipulation of microspheres and silicon nanowires to build 3-D micro/nanoscale structures in ambient conditions. Moreover, the capability of parallel nanomanipulation is certified by high-efficiency fabrication of a 2-D pattern with nanoparticles. Complicated micro/nanoscale manipulation and assembly can be reliably and efficiently performed using the proposed FRS.**

***Index Terms*—Atomic force microscope (AFM), flexible system, micro- and nanomanipulation, robot.**

I. Introduction

MICRO/NANOMANIPULATION and assembly covers applications from the micrometer to submicrometer and nanometer scale. These significant techniques have been widely used in the past decade for, e.g., micro/nanostructure assembly, material characterization, and biology manipulation. However, some aspects of the research on micro/nanomanipulation are still in their early stages. For instance, pick-and-place manipulation at the scale of several micrometers, submicrometers to nanometers is not yet well resolved, especially if the manipulation is performed under ambient conditions, which involves the presence of large adhesion forces, including van der Waals, electrostatic, and capillary forces [1]–[4]. In addition, manipulating efficiency is also another significant issue in micro/nanomanipulation research, for example, the state-of-the-art research on atomic force microscope (AFM) based nanomanipulation is still proving ineffective because of a serial imaging/manipulation process involved.

For building 2-D or 3-D microstructures and achieving biology micromanipulation, different microrobotic systems with various end effectors have been proposed [5]–[13]. However, few references in the literature report mechanical pick-and-place manipulation of microobjects with feature sizes of several micrometers in ambient conditions. When scaling down the manipulation size, nanoscale gripping can be performed in a vacuum (e.g., in scanning electron microscopes or transmission electron microscopes), where the often-predictable van der Waals force dominates interactions [14]–[17]. Nanoscale gripping can also be achieved using noncontact methods in a liquid, where influences from capillary forces are greatly reduced, e.g., optical tweezers [18], [19]. On the other hand, the AFM has been widely used in ambient environments for nanoscale manipulation and characterization. Nevertheless, its applications are generally restricted to the fabrication of 2-D nanopatterns or in-plane nanomaterial characterization through pushing or pulling operations on a single surface [20]–[24]. In order to build smart nanogrippers for 3-D nanomanipulation, a conceptual nanogripper constructed from two AFM cantilevers was first proposed [25], [26]. In ambient conditions, the AFM is undoubtedly a powerful scientific tool that not only provides a nanosample imaging capability, but is also a powerful tool for manipulation. Thus, a versatile AFM-based nanorobotic system might be a possible solution for achieving nanoscale to several micrometers scale pick-and-place in air.

Concerning the manipulation efficiency, an inherent limitation of conventional AFM-based nanomanipulation is that the AFM acts as an imaging sensor as well as a manipulation tool, hence cannot provide manipulation with visual feedback, but rather an insufficient serial process of scan–manipulation–scan. Haptic devices and virtual reality interfaces have been introduced into AFMs to facilitate nanomanipulation [27]–[29]. However, the serial operation is still required, thus making AFM nanomanipulation inefficient.

In this paper, based on our previous work [30]–[32], we present a concept to make a prototype of an AFM-based flexible robotic system (AFM-FRS) that is equipped with two collaborative cantilevers. By reconfiguring the modular hardware and software of the AFM-FRS, three different configurations can be obtained. With different manipulation strategies and protocols, two of the configurations can be respectively used to complete pick-and-place manipulations from the microscale of several micrometers to the nanoscale that are still challenges. In addition, the third system configuration of the AFM-FRS can be easily used for high-efficiency nanomanipulation by assigning imaging and 2-D pushing/pulling tasks in parallel to the individually actuated cantilevers. Automation on different applications could

Manuscript received June 23, 2009; revised October 5, 2009 and December 11, 2009. Recommended by Technical Editor N. Chaillet. This work was supported in part by the French Research Agency (ANR) through the NANOanalyse for micROmanipuLate Project under Grant PSIROB07-184846.

The authors are with the Institut des Systèmes Intelligents et Robotique, Université Pierre et Marie Curie/Unité Mixte de Recherche-Centre National de la Recherche Scientifique 7222, F-75005 Paris, France (e-mail: xie@isir.upmc.fr; stephane.regnier@upmc.fr).

Color versions of one or more of the figures in this paper are available online at http://ieeexplore.ieee.org.

Digital Object Identifier 10.1109/TMECH.2010.2040483

also be implemented, benefiting from accurate force sensing and positioning of the system.

The three kinematic configurations and necessities to reconfigure the AFM-FRS for multiscale applications are detailed. For automated parallel nanomanipulation, a dynamic pushing scheme with amplitude feedback, rather than the weak lateral force signal and the unstable normal force signal of the cantilever, is introduced for stable particle loss detection, and the shortest path solution was used for trajectory planning. Moreover, flexibilities and manipulation capabilities of the AFM-FRS are validated by performing three new experiments, including 3-D microsphere manipulation, nanowire pick-and-place, and nanoparticle parallel nanomanipulation on each corresponding system configuration. All the experiments, including tasks of manipulation and system reconfiguring, were carried out in a regular workday.

This paper is organized as follows. Section II introduces the prototype and experimental setup of the AFM-FRS. Various system configurations of the AFM-FRS are presented in Sections III– V. In Section VI, pick-and-place manipulation of microspheres and nanowires for building 3-D micro/nanostructures are performed using the AFM-FRS. Performance of the AFM-FRS was also validated by parallel imaging/manipulation of nanoparticles to form a nanopattern with a commonly used pushing manipulation. Section VII concludes the paper.

II. AFM-Based FRS

A. AFM-FRS Setup

Fig. 1(a) shows the AFM-FRS system setup, which is in the configuration for nanoscale pick-and-place. The system is equipped with an optical microscope and two sets of modules commonly used in a conventional AFM, mainly including two AFM cantilevers [namely, tip I and tip II, NANOSENSORS AdvancedTEC™ FM, see Fig. 1(b)], two sets of nanopositioning devices, and optical levers. The motion modules include an open-loop X–Y–Z piezoscanner (PI P-153.10H), an X–Y–Z closed-loop nanostage (MCL Nano-Bio2M on the X- and Y-axis, PI P–732.ZC on the Z-axis), an X–Y–Z motorized stage, and an X–Y–Z manual stage. Detailed specifications of the motion modules are summarized in Table I. Fig. 1(c) shows an optical microscope image of the collaborating tips in microsphere-grasping mode.

A data acquisition (NI 6289) card is used for high-speed (500∼800 Hz of sampling frequency for force and 600 kHz for amplitude) capture of the photodiode voltage output to estimate deflections on both tips induced by force loading or resonant oscillation. A multithread planning and control system based on the C++ is developed for AFM image scan and two-tip coordination control during manipulation. This control system enables programming of complex tasks on the highly distributed reconfigurable system.

B. Forces Calibration

Accurate interactive force detection between the AFM tips and the micro/nanoobjects or the micro/nanoenvironment is a prerequisite for achieving precise and stable manipulation. In our experiments, normal forces from both the tips are used to monitor the whole manipulation process, e.g., precise contact detection, grasping force sensing, and controlled nanoobject pushing.

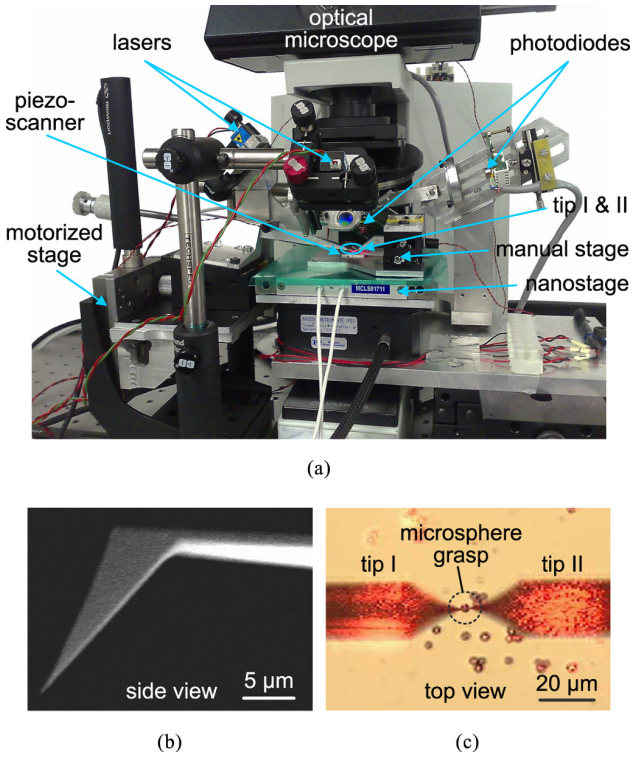

Fig. 1. (a) Photograph of the AFM-FRS on the configuration for nanoscale pick-and-place manipulation. (b) SEM image of the cantilever fabricated with a protruding tip. (c) Optical microscopic image of the collaborating tips in microsphere-grasping operation.

TABLE I
Specifications of Each Motion Module

Actuator	Travel range	Resolution
X-Y-Z piezoscanner	$10 \times 10 \times 10(\mu m)$	sub-nm
X-Y-Z nanostage	$50 \times 50 \times 10(\mu m)$	0.1 nm
X-Y-Z motorized stage	$25 \times 25 \times 25(mm)$	50 nm
X-Y-Z manual stage	$5 \times 5 \times 5(mm)$	0.5 μm

1) Normal Stiffness Calibration: The method of forced oscillation was first used to determine the thickness t of the cantilever from its natural frequency. As an Euler–Bernoulli beam, if resonant frequencies of the cantilever are known, its thickness t can be determined by

$$t = \frac{\omega_n}{K_n^2}\sqrt{\frac{12\rho}{E}} \tag{1}$$

where E and ρ are Young's modulus and the density of the cantilever, respectively, K_n is the wave number on the oscillating cantilever, and ω_n is the nth flexural resonant frequency. Set $n = 1$ for the first resonant mode, then $K_n l = 1.8751$, in which l is the cantilever length. The cantilever's normal stiffness k_n can be calculated by

$$k_n = \frac{Ewt^3}{4l^3} \tag{2}$$

TABLE II
NORMAL STIFFNESS AND FORCE CONVERSION FACTOR

Parameters	Tip I	Tip II
k_n	2.72 N/m	2.78 N/m
S_n	0.51 μm/V	0.49 μm/V
β	1.39 μN/V	1.36 μN/V

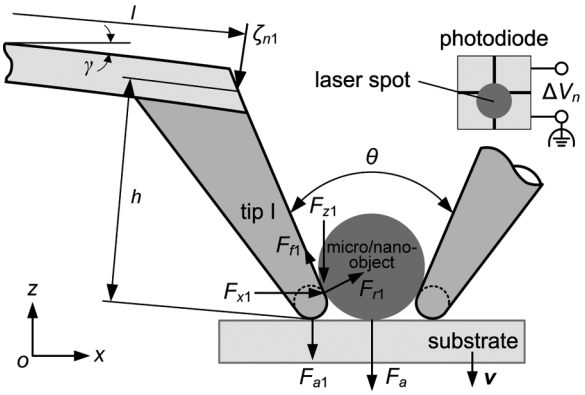

Fig. 2. Schematic diagram of the nanotip gripper and force simulation during the pickup manipulation.

where w is the width of the cantilever.

2) Normal Sensitivity of the Optical Lever: In order to convert signals from the optical levers into normal forces, it is necessary to calibrate the normal sensitivity of the optical lever S_n, and then, the normal force conversion factor $\beta = S_n k_n$, for which the corresponding bending force F_n is given by

$$F_n = \beta \Delta V_n \tag{3}$$

where ΔV_n represents the photodiode voltage output attributable to an applied force in the normal direction.

The normal stiffness of cantilevers and sensitivities of optical levers used in the experiments are shown in Table II.

C. Force Sensing During Pick-and-Place

Fig. 2 shows a schematic diagram of the nanotip gripper for the micro/nanoscale pick-and-place operation that has a clamping angle $\theta \approx 44^\circ$ micro/nanoscale pickup manipulation, for instance, interactive forces applied on tip I include repulsive forces F_{r1}, friction forces F_{f1}, and adhesive forces F_{a1}. The forces applied on tip I can be resolved into two components on the X-axis and the Z-axis in the defined frame, namely, F_{x1} and F_{z1}, respectively. F_{x1} is the clamping force that holds the micro/nanoobject. F_{z1} is the pickup force that balances adhesion forces from the substrate. To sense the pickup force, it is necessary to know the normal deflection on both cantilevers. The normal deflection ζ_{n1} associated with the normal voltage output of the optical lever on tip I is given by

$$\zeta_{n1} = \frac{F_{z1}\cos\gamma + F_{x1}\sin\gamma}{k_n} + \frac{F_{z1}\sin\gamma + F_{x1}\cos\gamma}{k_{xz}} \tag{4}$$

where γ is the mounting angle of the cantilever, and $k_{xz} = 2lk_n/3h$ is the bending stiffness due to the moment applied on the tip end, where h is the tip height. Assuming that the magnitude of F_{z1} and F_{x1} are of the same order, contributions from the F_{x1} to the normal deflection of tip I are relatively very small, since $k_{xz} \gg k_n$ and $\gamma = 5^\circ$. Therefore, the normal deflection induced from F_{z1} is only considered in the following calculations of the adhesion force F_a applied on the micro/nanoobject. Thus, F_{z1} can be simplified by estimating the normal voltage output ΔV_{n1} from the tip I as follows:

$$F_{z1} = \beta_1 \Delta V_{n1} \tag{5}$$

where β_1 is the normal force sensitivity of the optical lever. A similar pickup force F_{z2} can be also obtained on tip II. Before the gripper pulls off the substrate, the adhesion force F_a can be estimated as follows:

$$F_a = F_{z1} + F_{z2} = \beta_1 \Delta V_{n1} + \beta_2 \Delta V_{n2} - (F_{a1} + F_{a2}) \tag{6}$$

where β_2, ΔV_{n2}, and F_{a2} are the normal force sensitivity, normal voltage output, and adhesive force on tip II, respectively. Once the gripper pulls off the substrate, e.g., in the case of nanowire/tube pick-and-place, the adhesion force F_a is estimated as follows:

$$F_a = F_{z1} + F_{z2} = \beta_1 \Delta V_{n1} + \beta_2 \Delta V_{n2}. \tag{7}$$

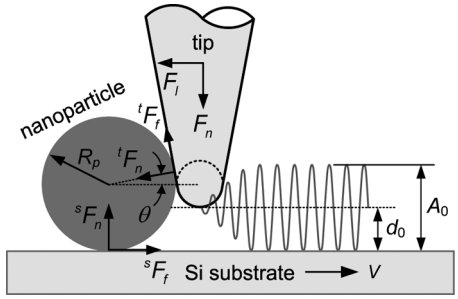

Fig. 3. Simulation of the pushing scheme and interaction forces during a nanoparticle push–slide operation.

D. Controlled Nanoparticle Pushing

As shown in Fig. 3, a constant distance d_0 between the tip and substrate is maintained during the nanoparticle push. In order to promptly detect the tip–nanoparticle contact as well as nanoparticle loss during particle push, the tip should be kept oscillating during the whole push procedure. Once contact with the nanoparticle is established, the amplitude of the oscillating tip fades from A_0 to zero. Contrariwise, the oscillating tip returns to the amplitude A_0 when the tip–nanoparticle contact is lost; this can be used to detect nanoparticle loss automatically to relocate the nanoparticle and restart the pushing operation.

Possible nanoparticle motion modes during the pushing operation are sliding, in-plane rotation, and out-of-plane rotation (rolling). Fig. 3 shows the interactive forces of the most common case of the push–slide motion. Let ${}^tF_f$ and ${}^tF_n$ be the friction and the normal force applied on the nanoparticle, respectively. For a successful push–slide operation, a threshold force along

the push direction is estimated as follows:

$$F_{\text{sliding}}^{\text{threshold}} = {}^{s}F_{f}^{\max} = {}^{t}F_{f}\sin\theta + {}^{t}F_{n}\cos\theta \tag{8}$$

$${}^{t}F_{f}^{\max} \geq F_{l}\sin\theta - F_{n}\cos\theta \tag{9}$$

where ${}^{s}F_{f}$ and ${}^{s}F_{n}$ are the friction force and the repulsive force applied on the nanoparticle from the substrate, respectively, and θ is the contact angle between the tip side and the nanoparticle. The minimum value of θ is equal to tip's half cone angle if the tip–substrate separation d_0 is small enough to make a contact with the tip's cone surface rather than tip's apex. F_l and F_n are the lateral and the normal forces applied on the tip from the cantilever, respectively. For low-speed and quasi-static pushing, it can be deduced that $F_l = {}^{s}F_f$ and $F_n = {}^{s}F_n$.

E. Piezoscanner Hysteresis and Creep Compensation

Motion coordination between two cantilevers is achieved by the closed-loop nanostage and the open-loop piezoscanner. Thus, piezoscanner hysteresis and creep should be well compensated, and both the stages should have the same displacement scale to ensure prompt and accurate positioning between both the tips and samples.

To characterize hysteresis and creep, the piezoscanner is fixed on the nanostage with the same axis arrangement in all the three spatial directions. The nanostage here is used as a reference stage, and the optical lever on tip I is used as a displacement sensor to measure the relative movement between the nanostage and the piezoscanner by lateral tracking well-defined slopes (AFM calibration grating TGF11) with the AFM tapping mode. During characterization, the piezoscanner is used to track the motion of the nanostage that provides a reference displacement due to the high resolution of the nanostage (0.1 nm) and the excellent dynamic performance of the piezoscanner (about 1 kHz on 1-μm motion amplitude). As the voltage–displacement response is characterized, the piezoscanner hysteresis and creep are predicated by Prandtl–Ishlinskii (PI) and logarithmic models, respectively [33]. After compensation, maximum errors on the full range of the X-axis, Y-axis, and the Z-axis are compressed from 28.14%, 27.82%, and 15.8% to 1.18%, 1.16%, and 0.97%, respectively.

III. Configuration of 3-D Micromanipulation

A. Overview

As the size of microobjects is reduced to several micrometers or submicrometers, following problems will arise with these conventional grippers. 1) Sticking phenomena becomes more severe due to the relatively larger contact area between the gripper and the microobject [2]. 2) The tip diameters of the microfabricated clamping jaws are comparable in size to the microobjects to be grasped. Conventional grippers are not geometrically sharp enough to pick up microobjects of several micrometers deposited on the substrate. Fortunately, the AFM tip has a very tiny apex (typically $\sim$10 nm in radius) with respect to the size of the microobject to be manipulated. Thus, the nanotip gripper can be used to achieve pick-and-place at the scale of several micrometers, since the contact area of the gripper–microobject is much smaller than the microobject–substrate contact. Moreover, real-time force sensing makes the manipulation more controllable.

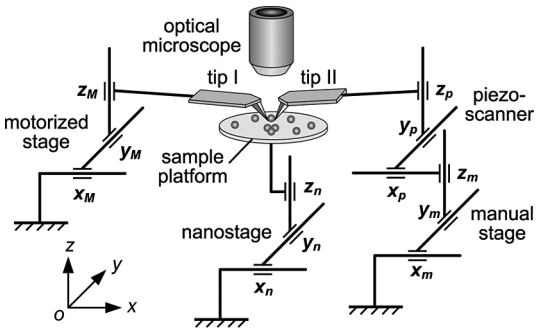

Fig. 4. Kinematic configuration of the AFM-RFS for 3-D micromanipulation at scale of several micrometers.

B. System Configuration for 3-D Micromanipulation

As shown in Fig. 4, the system configuration for 3-D micromanipulation is reconfigured as follows.

1) For a large manipulation travel range, the nanostage here is used to support the sample platform and transport the microobject during the manipulation.
2) Tip I, immovable during the pick-and-place micromanipulation, is fixed on the motorized stage for coarse positioning.
3) Tip II is actuated by the piezoscanner for gripper opening and closing operations. The piezoscanner is supported by the manual stage for coarse positioning.

C. Microscale Grasping Strategies

Benefiting from AFM-based accurate and stable amplitude feedback of a dithering cantilever, the grasping state can be successfully achieved by the amplitude feedback, with very weak interaction at the nano-Newton scale, protecting the fragile tips and the microobjects from damage during manipulation.

1) Grasping Points Search: As shown inset I of Fig. 5, the dithering cantilever with its first resonant mode is used to locate grasping points and detect contact. When approaching the microsphere with a separation between the tip and the substrate (typically 500 nm), the tip laterally sweeps the microsphere over the lower part of the microsphere. By this means, the grasping point can be accurately found by locating the minimum amplitude response of each single scan.

2) Contact Detection: From the scheme depicted in inset II of Fig. 5, the amplitude feedback is also used for contact detection. Tip–microsphere contact is detected as the amplitude reduces to a steady value close to zero.

D. 3-D Micromanipulation Protocol

As shown in Fig. 6, a protocol for pick-and-place microspheres mainly consists of the following four steps.

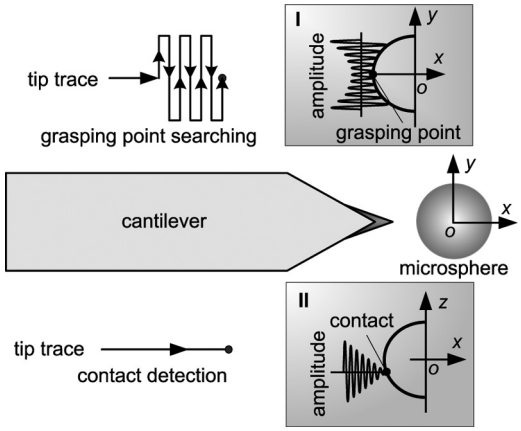

Fig. 5. Schematic diagrams for (inset I) grasping point searching and (inset II) contact detection with amplitude feedback of the dithering cantilever.

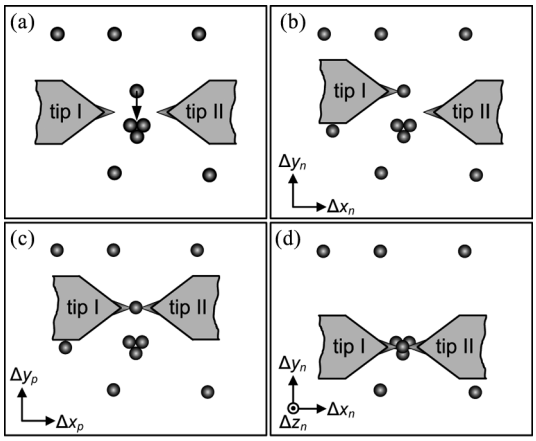

Fig. 6. Microsphere manipulation protocol. (a) Task planning. (b) Tip I and the microsphere are in contact. (c) Nanotip gripper is formed. (d) Pick up and release the microsphere to its target position.

1) System Initialization and Task Planning: Each axis of the nanostage and the piezoscanner are set in a proper position, thus supplying the manipulation with enough travel range on each axis. Then, the task is planned in Fig. 6(a) with a global view of the manipulation area that provides coarse positions of the microspheres and tips.

2) Making Tip I Microsphere in Contact: In Fig. 6(b), tip I is started to approach the microsphere by moving the nanostage with amplitude feedback to search for the grasping point and detect contact.

3) Forming the Gripper: Similarly, tip II approaches the microsphere by moving the piezoscanner. Once tip II and the microsphere are in contact, a nanotip gripper is configured in Fig. 6(c) for a manipulation.

4) Pick-and-Place Micromanipulation: In Fig. 6(d), the microsphere is picked up, transported, and released by moving the nanostage with a proper displacement on each axis that depends on the diameter of the microsphere and its destination. The whole process of 3-D micromanipulation is monitored by real-time force sensing.

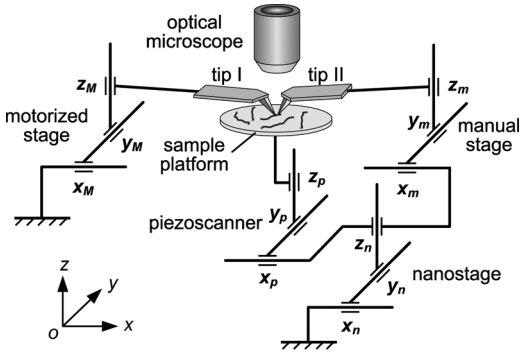

Fig. 7. Kinematic configuration of the AFM-RFS for nanoscale pick-and-place.

IV. Configuration of 3-D Nanomanipulation

A. Overview

In addition to the microscale pick-and-place, the proposed nanotip gripper can also be used to achieve nanoscale pick-and-place in ambient conditions, since the tiny tip is geometrically sharp enough to pick up nanoobjects deposited on the substrate, and simultaneously has capabilities of sensing nanoscale force between the nanoobject and the tool. Moreover, the nanotip gripper itself acts as an image sensor for nanoobject positioning.

B. System Configuration for 3-D Nanomanipulation

Compared with the 3-D micromanipulation, tip alignment precision is the key factor in succeeding the nanoscale pick-and-place. Therefore, the closed-loop nanostage is considered in this configuration for accurate tip alignment. As shown in Fig. 7, the system configuration for 3-D nanomanipulation is reconfigured as follows.

1) The nanostage is used for image scan with tip I.
2) Nanoobjects are supported and transported by the piezoscanner.
3) Tip I, fixed on the motorized stage for coarse positioning, is immovable during the pick-and-place micromanipulation. Before manipulation, cantilever I acts as an image sensor for nanoobject positioning.
4) For accurate gripper alignment between tip I and tip II, tip II is fixed on the nanostage rather than the piezoscanner. Tip II is supported by the manual stage for coarse positioning.

C. 3-D Nanomanipulation Protocol

Nanowires and nanotubes are being intensively investigated. Thus, a protocol is developed here for nanowire or nanotube pick-and-place. However, applications can easily be extended to, for example, pick-and-place of nanorods or nanoparticles dispersed on a substrate.

1) System Initialization: Once the manipulation area is selected under the optical microscope, both the tips are aligned as a quasi-gripper above the center of the manipulation area. Each axis of the nanostage and the piezoscanner is initialized at an

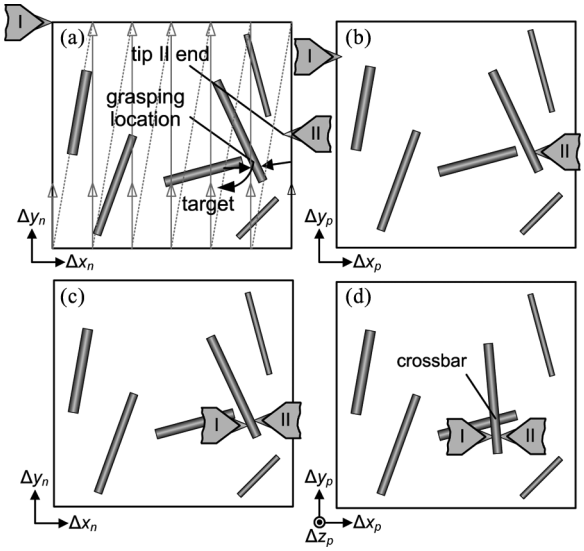

Fig. 8. Protocol for nanowire pick-and-place. (a) Image scan for task planning. (b) Tip II is in contact with the nanowire. (c) Tip I is in contact with the nanowire, thus forming a nanotip gripper. (d) Pick up and release a nanowire to its target position.

appropriate position to allow for enough manipulation motion travel.

2) Image Scan for Task Planning: In this step, tip I is used to fully scan the relevant area obtaining a topographic image that contains nanoobjects to be manipulated and the end of tip II. Fig. 8(a) shows a simulated image that contains the topography of two nanowires and the end of tip II. The image provides the following pick-and-place with relative positions between tip I, tip II, and the nanoobjects to be manipulated. However, after a long period image scan, relocating tip II is recommenced to eliminate system's thermal drift.

3) Making Tip II Nanowire in Contact: As shown in Fig. 8(b), tip II approaches the nanowire to make contact by moving the X-axis of the piezoscanner. A gap (typically $\sim$20 nm above the snap-in boundary) between tip II and the substrate should be maintained during the approach to enable a negative deflection response in the form of a tiny force applied on tip II, and hence, sensitive detection of the tip–nanowire contact.

4) Forming the Gripper: Similarly, in Fig. 8(c), once tip I is in contact with the nanowire, a nanotip gripper is configured for pick-and-place manipulation of the nanowire.

5) Pick-and-Place Nanomanipulation: The nanotip gripper in this step is used to pick up, transport, and release the nanowire to its target position by moving the piezoscanner on the X-, Y-, or Z-axis. The displacement on each axis depends on the dimensions of the nanowire and the location of the destination. Fig. 8(d) shows a simulated postmanipulation image, in which a nanowire crossbar is built. The complete pick-and-place procedure is monitored by force sensing.

V. Configuration for Parallel Nanomanipulation

A. Overview

Conventional AFM-based manipulation has an inefficient scan–manipulation–scan process, which make mass production impossible. Fortunately, the AFM-FRS has two individually actuated cantilevers that can be used simultaneously as an image sensor and manipulation tool, respectively. By this means, image scan and nanomanipulation can be performed in parallel.

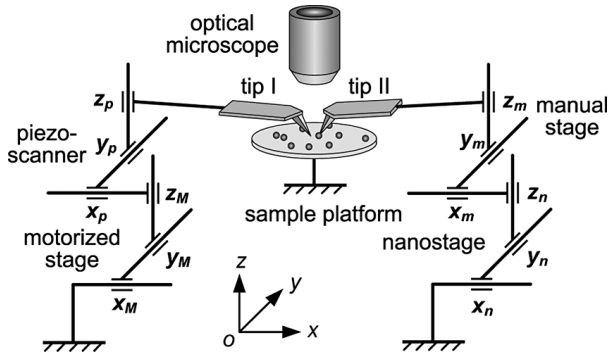

Fig. 9. Kinematic configuration of the AFM-RFS for parallel imaging/nanomanipulation.

B. System Configuration for Parallel Nanomanipulation

Position precision is one of the critical issues in the AFM-based 2-D nanomanipulation. Among several factors that cause positioning errors, the most significant are piezoscanner hysteresis and creep. Thus, the closed-loop nanostage in this configuration is used to actuate the manipulating tip. As shown in Fig. 9, the system configuration for parallel nanomanipulation is reconfigured as follows.

1) Tip I, used as image sensor, is actuated by the piezoscanner that is fixed on the motorized stage for coarse positioning. Excellent image quality can be obtained, even though the scan length on tip II is more than 300 nm, which is sufficient for tip positioning with a dynamic image display updated by real-time scanning data.
2) To minimize positioning errors for a efficient manipulation, tip II, used as an end effector for nanoobjects manipulation, is actuated by the nanostage rather than the piezoscanner. The manual stage is used here for coarse positioning.
3) The sample platform is immovable during the manipulation and fixed on the system base.
4) The action of each cantilever is controlled by the independent thread of the control system and the image scanning data are shared by these two threads.

C. Parallel Nanomanipulation Scheme

Fig. 10 is a diagram of the parallel image/manipulation with image scan using tip I. After system initialization, local scan is started to locate tip II with tip I. Once tip II locating is completed, two parallel threads are activated to control a parallel imaging/manipulation task. One is used for imaging with tip I to perform a full scan of the pertinent area, thus resulting in a topographic image that contains nanoobjects to be manipulated as well as the end of tip II (as seen in the simulated image

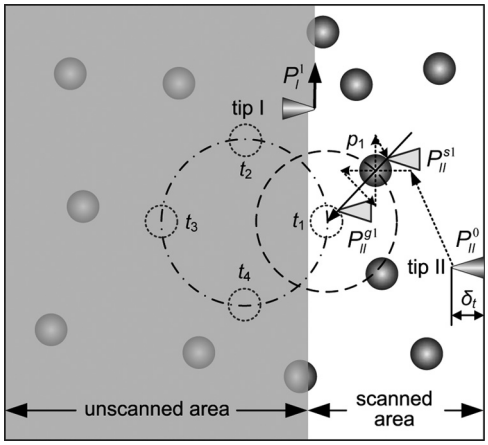

Fig. 10. Task planning scheme for the parallel imaging/nanomanipulation with the shortest path solution.

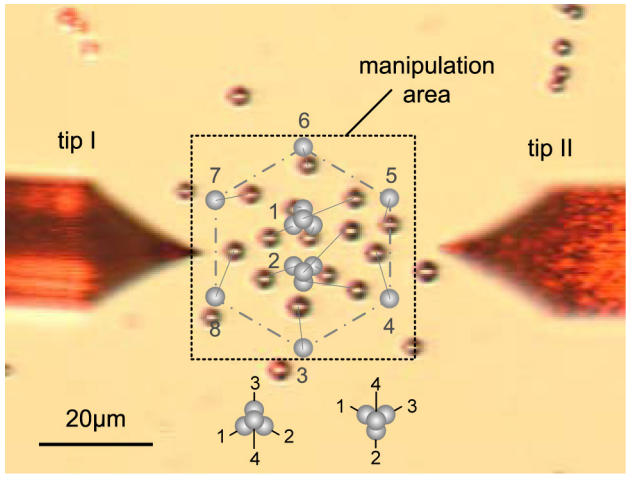

Fig. 11. Task descriptions of the microsphere assembly. A micropattern formed by a regular hexagon and two micropyramids are planned. Assembly sequences are described by numbers.

at position P_{II}^{0}). The second thread is assigned to manage the performance of tip II, which is in idle process until first target position t_1 is entirely covered by the scanned area when tip I reaches position P_{I}^{1}.

The shortest path resolution with linear trajectories is used to choose a corresponding particle to target t_1. As seen the Fig. 10, particle p_1, which is with the shortest distance to t_1 compared with others scanned particles, is first pushed. The manipulation task is activated after the coarse positioning of particle p_1 by processing the scanned image. Accurate center position of particle p_1 are further obtained by locally scanning the nanoparticle horizontally and vertically with tip II along a defined line. When tip II reaches point P_{II}^{s1} on the pushing line, the push is started until tip II reaches P_{II}^{g1}, where particle p_1 has been pushed to its target position t_1. After the first manipulation, tip II is set to the idle process again, until target position t_2 emerges within the dynamic image.

D. Parallel Manipulation Efficiency

Task time of the parallel imaging/manipulation operation can be given as follows:

$$t_{\mathrm{task}} = \max(t_s, t_m) + t_s \tag{10}$$

where t_s is the scanning time of one image frame and t_m is the total manipulation time estimated from the sum of manipulation time of each single nanoobject. For the normal-speed AFM, t_{task} is often equal to $2t_s$, except for a complex manipulation task that cannot be fulfilled within one frame period, and so has task time of $t_m + t_s$. This scheme can save a lot of time compared with the serial imaging/manipulation operation that has task time of $t_m + 2t_s$. One disadvantage of this scheme is that environment-based motion planning is unavailable during the manipulation. However, parallel imaging/manipulation can be perfectly performed by this scheme if a manipulation objective is defined before the operation.

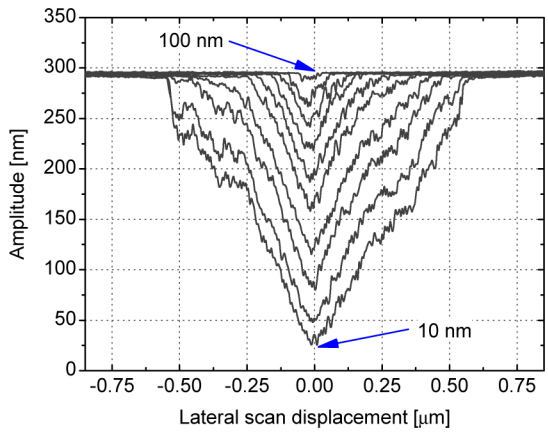

Fig. 12. Amplitude responses on tip II when searching the grasping points.

VI. Experimental Results

A. 3-D Microsphere Assembly

1) Task Description: Nylon microspheres with diameter of about 3∼4 μm were manipulated to build 3-D microstructures in experiments. The microspheres were deposited on a freshly cleaned glass slide, and then, an area of interest was selected under the optical microscope. Fig. 11 shows a plan view of the selected area, in which 14 microspheres separated in a 50-μm square frame are going to be manipulated to build two 3-D micropyramids and a regular 2-D hexagon labeled by assembly sequences from 1 to 8. Each pyramid is constructed from four microspheres with two layers, and the assembly sequences are shown in the bottom insets for two different arrangements of the pyramids.

2) Force Sensing during Micromanipulation: Fig. 12 shows a result of grasping point searching, in which the dithering tip II laterally sweeps the microsphere within a range of 1.75 μm on the y-axis and with a free oscillating amplitude of about 285 nm. Ten different distances to the microsphere were tested from 100 to 10 nm with an interval of 10 nm, and consequently, the

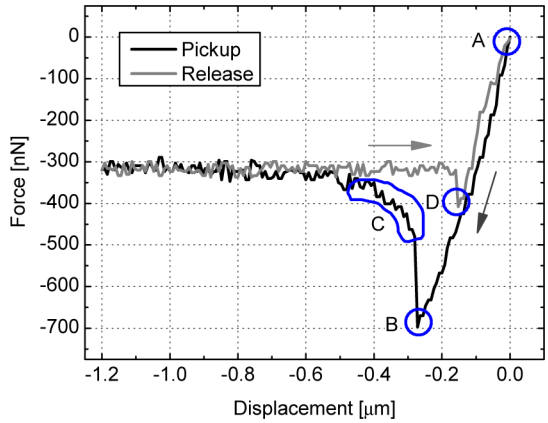

Fig. 13. Synthesized normal force responses from both the tips in the pick-and-place micromanipulation.

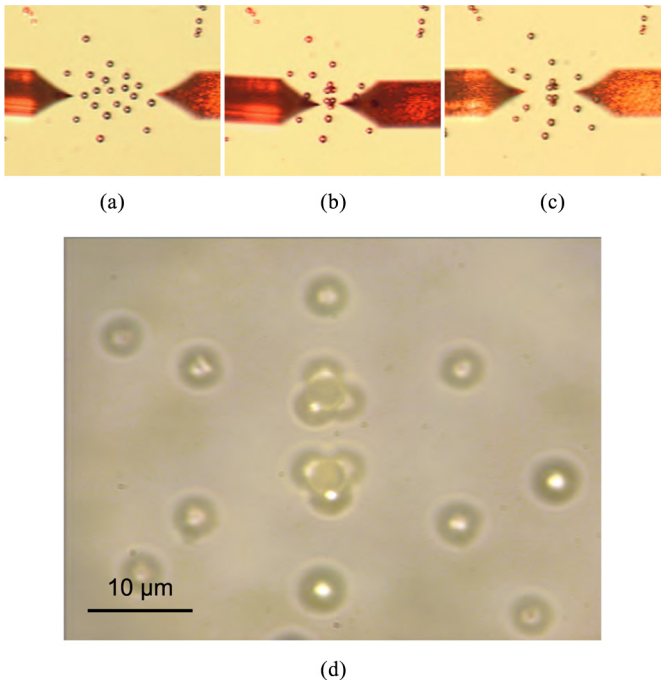

Fig. 14. Microassembly result shows that two micropyramids and a regular hexagon have been built. (a) Before the microassembly. (b) Micropyramids were built. (c) After the microassembly. (d) Enlarged image of the microassembly result under a magnification of 100×.

grasping point is well located with an accuracy of ±10 nm. Fig. 13 shows a full force spectroscopy curve during the pick-and-place of a microsphere deposited on a glass slide with an ambient temperature of 20 °C and relative humidity of 40%. In this curve, point A represents the start of the pick-and-place, point B represents the pull-off location of the microsphere–substrate contact, point C represents nonlinear force restitution due to the tip–microsphere frictions, and point D represents the snap-in point between the microsphere and the substrate. The force spectroscopy curve is synthesized from force responses on tip I and tip II.

3) 3-D Micromanipulation Results: Fig. 14 shows an automated microassembly result consisting of two 3-D micropyramids and a 2-D pattern of a regular hexagon. The whole manipulation process was completed in 11 min; therefore, the average manipulation time for each microsphere is about 47 s, which mainly breaks down into about 20 s for microsphere grasping including the grasping point search and contact detection processes using amplitude feedback, 10∼35 s for microsphere release and, the remaining time for transport.

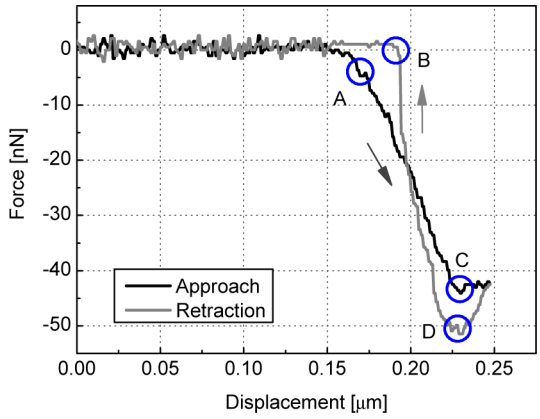

Fig. 15. Contact detection on the SiNW with tip II.

Assembly of the fourth microsphere is the key to success in building a micropyramid. During pick-and-place of the fourth microsphere, microscopic vision was first used for coarse positioning the target, and then, the normal force feedback of the gripper was used to detect the vertical contact between the fourth microsphere and other three microspheres on the base. When the contact is established, a small vertical force was applied on the fourth microsphere by moving the nanostage upward and it will adjust to contact with all the base microspheres.

B. 3-D Silicon Nanowire (SiNW) Assembly

1) Sample Preparation: In experiments, SiNWs were deposited on a freshly cleaned silicon wafer coated with 300-nm silicon dioxide. AFM images show that the SiNWs have a taper shape and have diameters of 25 nm (top) ∼200 nm (root) and lengths of about 4∼7 μm.

2) Force Sensing during Nanomanipulation: Fig. 15 shows an example of the contact detection with tip II; point A and point C are where the tip contacts with the SiNW and the Si substrate, respectively; point B and point D are where the tip breaks the contact with the Si substrate and the SiNW, respectively. Fig. 16 shows a curve of the peeling force spectroscopy on tip II for the pick-and-place manipulation of the SiNW; point A and point B are where the tip snaps in and pulls off the Si substrate, respectively. The shape of curve of the force responses on tip I are similar, except for the force magnitude due to different force sensitivities on each tip and uneven grasping due to asymmetric alignment of the SiNW relative to the grasping direction. This force spectroscopy during the pickup operation shows stable grasping for further SiNW transport.

3) 3-D Nanomanipulation Results: Fig. 17 shows an experimental result of 3-D SiNW manipulation. A prescanned image (9 μm × 9 μm) is shown in Fig. 17(a), which includes the

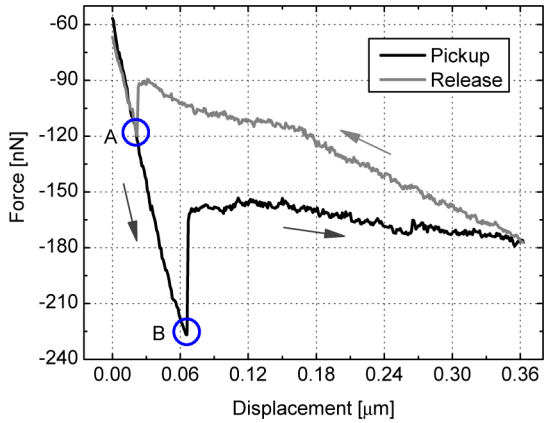

Fig. 16. Force detection on tip II during the pick-and-place nanomanipulation of the SiNW.

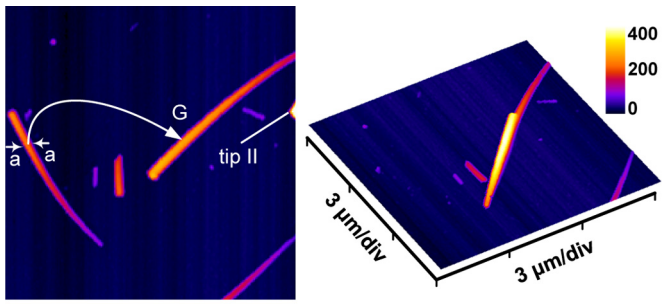

Fig. 17. Pick-and-place results of the SiNWs. (a) A prescanned image in which a–a and G are the grasping location and the target position, respectively. (b) A postmanipulation image verifies that the manipulated SiNW is piled upon another nanowire deposited on the Si substrate.

topographic image of SiNWs and the local image of tip II. A grasping location of the nanowire to be manipulated is marked with a–a, where the SiNW has a height of 160 nm. Fig. 17(b) is a postmanipulation image. It can be seen that the SiNW has been successfully transported and piled onto another SiNW. The manipulation procedure is described as follows. Once the SiNW was reliably grasped, the piezoscanner moved down 560 nm at a velocity of 80 nm/s. In this step, the SiNW was transported a distance of 4.4 μm along the X-axis at a velocity of 120 nm/s and 0.12 μm along the Y-axis at a lower velocity of 3.3 nm/s. In the releasing step, the piezoscanner moved up at a velocity of 100 nm/s. As tip II was slightly bent upward leading to a positive response of 0.015 V, tip I and tip II were separated by moving both the nanostage and the piezoscanner on the X-axis to release the SiNW from the nanotip gripper.

C. Parallel Imaging/Nanomanipulation of Nanoparticles

1) Sample Preparation: The manipulation samples were prepared by depositing 50-nm gold colloidal particles (Ted Pella, Inc.) from aqueous solution on a freshly cleaned silicon substrate using the boiling method [34]. The silicon substrate was placed on a hot plate that was set at an appropriate temperature of about 100∼110 °C. Drops of the gold nanoparticle solution were released on the hot substrate and were left to boil.

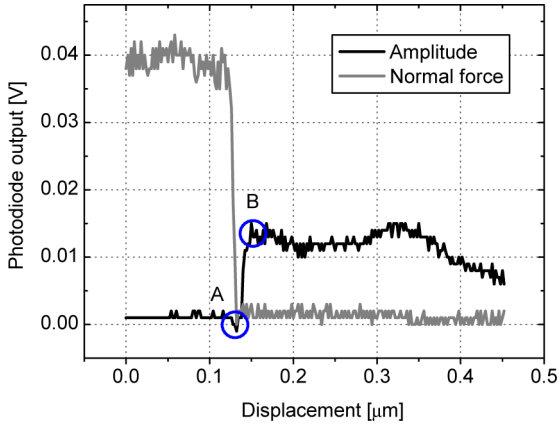

Fig. 18. Example of the normal force and amplitude responses during a particle push.

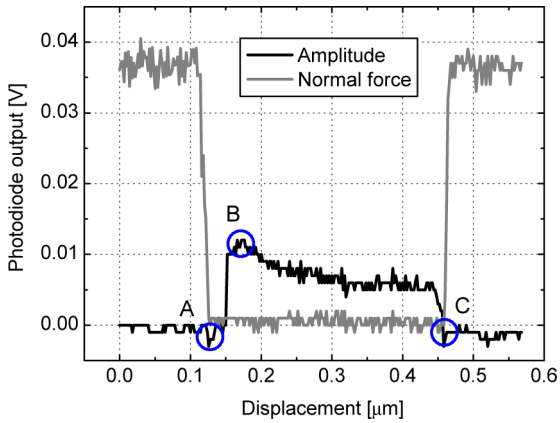

Fig. 19. Example of the normal force and amplitude responses during a particle push followed by particle loss.

2) Particle Loss Detection: First, a contact point positioning error leads to contact loss during the push manipulation due to nanoparticle in-plane rotation, especially over a long distance push. In order to detect particle loss promptly, tip II is kept in oscillating mode during the whole push procedure. Fig. 18 shows an example of the normal force and amplitude responses in the cases of successful push; point A shows the tip snaps into contact with a nanoparticle, and point B indicates motion occurs when the static friction is broken. Fig. 19 shows a cases of nanoparticle loss, where point A shows the tip and nanoparticle snap into contact. Motion occurs at point B and the particle loss occurs at point C. By this means, not only can the tip–nanoparticle contact be detected by amplitude fading, but also the particle loss when the amplitude suddenly increases from zero.

3) Parallel Nanomanipulation Results: A parallel image/manipulation task was performed with normal-speed image scan. In Fig. 20(a), five gold nanoparticles with a diameter of 50 nm and the corresponding target positions emerged on the dynamic image I–III in sequence. In Fig. 20(b), selected particles were pushed onto the corners and the middle of a square within the image scan period. The imaging frame period t_s was about 8 min. In contrast, the total manipulation time t_m for these

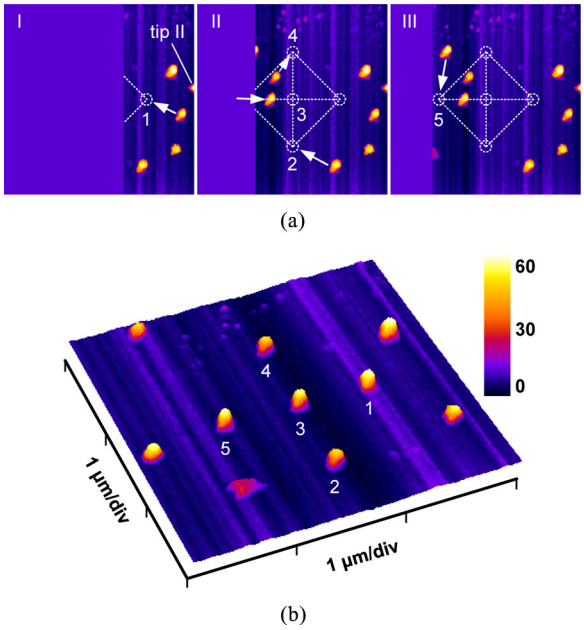

Fig. 20. Parallel imaging/manipulation result with a normal-speed image scan of tip I. (a) Emergences of five particles (50 nm in diameter) and targets on three different dynamic displays I to III. (b) Five nanoparticles were pushed to form a square pattern with a central particle.

five nanoparticles was less than three and a half minutes with a pushing velocity of 200 nm/s. The result indicates that a more complicated task can be performed within an imaging period in order to increase AFM-based nanomanipulation efficiency and make the mass production feasible.

VII. Conclusion

We have developed an AFM-FRS for multiscale micro/nanomanipulation and assembly applications. Using AFM-based accurate force sensing and the tiny apex of the AFM tip, a nanotip gripper, which is able to pick-and-place very tiny samples, was constructed from two tips fitted to the AFM-FRS. Using this nanotip gripper, 3-D manipulation from the nanoscale to the scale of several micrometers was achieved. Moreover, the two-tip configuration of the AFM-FRS also makes high-efficiency parallel imaging/nanomanipulation feasible by performing imaging and manipulation in parallel. Three different configurations and corresponding experiments, respectively, for 3-D microsphere manipulation, 3-D nanowire manipulation, and parallel nanomanipulation of nanoparticles, were presented in detail. As a result, the AFM-FRS makes applications from the microscale to the nanoscale on the same FRS practical, such as building micro/nano 3-D structures and devices, and high-throughput 2-D nanomanipulation.

Acknowledgment

The authors would like to thank Prof. D. S. Haliyo for the valuable discussions.

References

[1] Y. Rollot, S. Régnier, and J. C. Guinot, "Simulation of micro-manipulations: Adhesion forces and specific dynamic models," *Int. J. Adhes. Adhes.*, vol. 19, no. 1, pp. 35–48, 1999.

[2] A. Menciassi, A. Eisinberg, I. Izzo, and P. Dario, "From 'macro' to 'micro' manipulation: Models and experiments," *IEEE/ASME Trans. Mechatronics*, vol. 9, no. 2, pp. 311–320, Jun. 2004.

[3] L. X. Dong and B. J. Nelson, "Robotics in the Small," *IEEE Robot. Autom. Mag.*, vol. 14, no. 3, pp. 111–121, Jun. 2007.

[4] M. Savia and H. N. Koivo, "Contact micromanipulation—Survey of strategies," *IEEE/ASME Trans. Mechatronics*, vol. 14, no. 4, pp. 504–514, Aug. 2009.

[5] O. Millet, P. Bernardoni, S. Régnier, P. Bidaud, E. Tsitsiris, D. Collard, and L. Buchaillot, "Electrostatic actuated micro gripper using an amplification mechanism," *Sens. Actuator A, Phys.*, vol. 114, no. 2–3, pp. 371–378, 2004.

[6] R. Pérez, J. Agnus, C. Clévy, A. Hubert, and N. Chaillet, "Modeling, fabrication, and validation of a high-performance 2-DoF piezoactuator for micromanipulation," *IEEE/ASME Trans. Mechatronics*, vol. 10, no. 2, pp. 161–171, Apr. 2005.

[7] W. Driesen, T. Varidel, S. Régnier, and J. M. Breguet, "Micromanipulation by adhesion with two collaborating mobile micro robots," *J. Micromech. Microeng.*, vol. 15, no. 10, pp. S259–S267, 2005.

[8] A. Neild, S. Oberti, F. Beyeler, J. Dual, and B. J. Nelson, "A micro-particle positioning technique combining an ultrasonic manipulator and a microgripper," *J. Micromech. Microeng.*, vol. 16, no. 8, pp. 1562–1571, 2006.

[9] C. D. Onal and M. Sitti, "Visual servoing-based autonomous 2-D manipulation of microparticles using a nanoprobe," *IEEE Trans. Control Syst. Tech.*, vol. 15, no. 5, pp. 842–852, Sep. 2007.

[10] K. Y. Kim, X. Y. Liu, Y. Zhang, and Y. Sun, "Nanonewton force-controlled manipulation of biological cells using a monolithic MEMS microgripper with two-axis force feedback," *J. Micromech. Microeng.*, vol. 18, no. 5, pp. 055013-1–055013-8, 2008.

[11] B. L. Walle, M. Gauthier, and N. Chaillet, "Principle of a submerged freeze gripper for microassembly," *IEEE Trans. Robot.*, vol. 24, no. 4, pp. 897–902, Aug. 2008.

[12] C. Elbuken, M. B. Khamesee, and M. Yavuz, "Design and implementation of a micromanipulation system using a magnetically levitated MEMS robot," *IEEE/ASME Trans. Mechatronics*, vol. 14, no. 4, pp. 434–445, Aug. 2009.

[13] H. C. Liaw and B. Shirinzadeh, "Neural network motion tracking control of piezo-actuated flexure-based mechanisms for micro-/nanomanipulation," *IEEE/ASME Trans. Mechatronics*, vol. 14, no. 5, pp. 517–527, Oct. 2009.

[14] T. Fukuda, F. Arai, and L. X. Dong, "Assembly of nanodevices with carbon nanotubes through nanorobotic manipulations," *Proc. IEEE*, vol. 91, no. 11, pp. 1803–1818, Nov. 2003.

[15] K. Molhave, T. Wich, A. Kortschack, and P. Boggild, "Pick-and-place nanomanipulation using microfabricated grippers," *Nanotechnology*, vol. 17, no. 10, pp. 2434–2441, 2006.

[16] L. X. Dong, F. Arai, and T. Fukuda, "Destructive constructions of nanostructures with carbon nanotubes through nanorobotic manipulation," *IEEE/ASME Trans. Mechatronics*, vol. 9, no. 2, pp. 350–357, Jun. 2004.

[17] S. Fatikow, T. Wich, H. Hulsen, T. Sievers, and M. Jahnisch, "Microrobot system for automatic nanohandling inside a scanning electron microscope," *IEEE/ASME Trans. Mechatronics*, vol. 12, no. 3, pp. 244–252, Jun. 2007.

[18] L. Bosanac, T. Aabo, P. M. Bendix, and L. B. Oddershede, "Efficient optical trapping and visualization of silver nanoparticles," *Nano Lett.*, vol. 8, no. 5, pp. 1486–1491, 2008.

[19] C. Pacoret, R. Bowman, G. Gibson, S. Haliyo, D. Carberry, A. Bergander, S. Régnier, and M. Padgett, "Touching the microworld with force-feedback optical tweezers," *Opt. Exp.*, vol. 17, no. 12, pp. 10260–10264, 2009.

[20] M. Sitti and H. Hashimoto, "Controlled pushing of nanoparticles: Modeling and experiments," *IEEE/ASME Trans. Mechatronics*, vol. 5, no. 2, pp. 199–211, Jun. 2000.

[21] M. Guthold, M. R. Falvo, W. G. Matthews, S. Paulson, S. Washburn, D. A. Erie, R. Superfine, F. P. Brooks, and R. M. Taylor, "Controlled manipulation of molecular samples with the nanomanipulator," *IEEE/ASME Trans. Mechatronics*, vol. 5, no. 2, pp. 189–198, Jun. 2000.

[22] R. Resch, D. Lewis, S. Meltzer, N. Montoya, B. E. Koel, A. Madhukar, A. A. G. Requicha, and P. Will, "Manipulation of gold nanoparticles in liquid environments using scanning force microscopy," *Ultramicroscopy*, vol. 82, no. 1–4, pp. 135–139, 2000.

[23] M. Sitti, "Atomic force microscope probe based controlled pushing for nanotribological characterization," *IEEE/ASME Trans. Mechatronics*, vol. 9, no. 2, pp. 343–349, Jun. 2004.
[24] Y. J. Yun, C. S. Ah, S. Kim, W. S. Yun, B. C. Park, and D. H. Ha, "Manipulation of freestanding Au nanogears using an atomic force microscope," *Nanotechnology*, vol. 18, no. 50, pp. 505304-1–505304-5, 2007.
[25] M. Sitti, B. Aruk, K. Shintani, and H. Hashimoto, "Scaled teleoperation system for nanoscale interaction and manipulation," *Adv. Robot.*, vol. 17, no. 3, pp. 275–291, 2003.
[26] M. Sitti, "Teleoperated 2-d micro/nanomanipulation using an atomic force microscope," Ph.D. dissertation, Univ. Tokyo, Tokyo, Japan, Sep. 1999.
[27] M. Sitti and H. Hashimoto, "Teleoperated touch feedback of surfaces at the nanoscale: Modeling and experiments," *IEEE/ASME Trans. Mechatronics*, vol. 8, no. 2, pp. 287–298, Jun. 2003.
[28] G. Y. Li, N. Xi, M. M. Yu, and W. K. Fung, "Development of augmented reality system for AFM-based nanomanipulation," *IEEE/ASME Trans. Mechatronics*, vol. 9, no. 2, pp. 358–365, Jun. 2004.
[29] L. Q. Liu, Y. L. Luo, N. Xi, Y. C. Wang, J. B. Zhang, and G. Y. Li, "Sensor referenced real-time videolization of atomic force microscopy for nanomanipulations," *IEEE/ASME Trans. Mechatronics*, vol. 13, no. 1, pp. 76–85, Feb. 2008.
[30] H. Xie and S. Régnier, "Three-dimensional automated micromanipulation using a nanotip gripper with multi-feedback," *J. Micromech. Microeng.*, vol. 19, no. 7, pp. 075009-1–075009-9, 2009.
[31] H. Xie, S. Haliyo, and S. Régnier, "A versatile atomic force microscope for three-dimensional nanomanipulation and nanoassembly," *Nanotechnology*, vol. 20, no. 21, pp. 215301-1–215301-9, 2009.
[32] H. Xie, S. Haliyo, and S. Régnier, "Parallel imaging/manipulation force microscopy," *Appl. Phy. Lett.*, vol. 94, no. 15, pp. 153106-1–153106-3, 2009.
[33] H. Xie, M. Rakotondrabe, and S. Régnier, "Characterization of the piezoscanner with an optical lever and a reference nanopositioning stage," *Rev. Sci. Instrum.*, vol. 80, no. 4, p. 046102, 2009.
[34] K. Lee, M. Duchamp, G. Kulik, A. Magrez, J. W. Seo, S. Jeney, A. J. Kulik, and L. Forro, "Uniformly dispersed deposition of colloidal nanoparticles and nanowires by boiling," *Appl. Phys. Lett.*, vol. 91, no. 17, pp. 173112-1–173112-3, 2007.

Hui Xie (S'05–M'07) received the B.S. degree in mechanical engineering from Harbin University of Science and Technology, Harbin, China, in 2000, and the M.S. degree in mechanical engineering and the Ph.D. degree in mechatronics engineering from Harbin Institute of Technology, Harbin, in 2002 and 2006, respectively.

In 2003, he was a Research Assistant in the State Key Laboratory of Robotics and System, Harbin Institute of Technology, where he was a Lecturer in 2005. Since December 2008, he has been a Research Associate at the Institut des Systèmes Intelligents et Robotique, Université Pierre et Marie Curie/Centre National de la Recherche Scientifique, Paris, France, where he was a Postdoctoral Researcher beginning in December 2006. His current research interests include microrobotics/nanorobotics, microscopic vision and automation on atomic-force-microscope-based nanomanipulation, parallel nanomanipulation force microscopy, and 3-D nanomanipulation force microscopy.

Dr. Xie was the recipient of the Best Application Paper Award at the IEEE/RSJ International Conference on Intelligent Robots and Systems in 2009 and also the Toshio Fukuda Best Paper Award in Mechatronics–Finalists at the IEEE International Conference on Mechatronics and Automation in 2005.

Stéphane Régnier received the Ph.D. degree in mechanics and robotics from the University of Pierre and Marie Curie, Paris, France, in 1996.

He is currently a Professor in the Institute of Institut des Systèmes Intelligents et Robotique (ISIR), University of Pierre & Marie Curie, where he has been the Head of the ISIR Micromanipulation Team since 2001. His research interests include micro and nanomanipulation, teleoperation and haptic feedback at the nanoscale, micromechatronics, and biological cell characterization.